Journal of the European Ceramic Society 22 (2002) 191–198

www.elsevier.com/locate/jeurceramsoc

ZrO_2–Al_2O_3 eutectic plates produced by laser zone melting

A. Larrea*, G.F. de la Fuente, R.I. Merino, V.M. Orera

Instituto de Ciencia de Materiales de Aragón, Consejo Superior de Investigaciones Científicas-Universidad de Zaragoza, c/ María de Luna 3, E-50015 Zaragoza, Spain

Received 30 November 2000; accepted 26 March 2001

Abstract

This paper describes a procedure for preparing large surfaces of eutectic composites directionally solidified from the melt, with very fine and uniform microstructures. Large surface plates of the Al_2O_3–ZrO_2 eutectic, with thickness up to 250 μm, have been grown by solidification using a modified laser zone melting method suitable for the preparation of large area samples. The surface of a ceramic precursor is scanned with a rectangular CO_2 laser beam of 20×0.5 mm^2 size which induces surface melting. The resulting microstructure is colony free and it consists of fine and alternating interpenetrating Al_2O_3 and ZrO_2 single crystal lamellae. This microstructure is the basis for improvement of mechanical behaviour in the processed material. The interspacing, crystal structure and orientation relationship between the phases has been determined. Solidification fronts were studied as a function of the processing conditions. A mapping of the residual stresses has also been performed along the transverse plate sections using micro-luminescence techniques.

Keywords: Al_2O_3; Composites; Laminates; Laser-zone-melting; Microstructure; ZrO_2-Al_2O_3

1. Introduction

Lasers have been widely used in material processing for almost the last three decades. Most of the applications of laser processing are based upon the thermal effects caused by the laser radiation absorbed by the material. The heat generated produces microstructural and even structural changes. Control of laser heating parameters such as laser beam shape, wavelength, power, etc., is essential for these applications.

Directional solidification of high melting temperature compounds is an important example of the application of the laser heating technique. Oxide single crystals are now currently grown using the laser float zone method (LFZ) where the melt volume is self-confined by the surface tension of the liquid. Advantages of this method rely on the absence of any container or die avoiding possible sources of contamination and allowing for very high liquid temperatures. An added advantage of the LFZ technique is the possibility of having planar and stable liquid–solid interfaces through which high thermal gradients are established, hence allowing for high crystal growth rates.

Recently, LFZ has also been successfully used to grow solidified oxide eutectic composites with ordered microstructures. These composites, known as melt growth composites (MGCs), are in situ composite materials with a novel and very fine microstructure (in the micron range) which may combine the characteristics of each constituent to optimise the performance and properties of the composite.[1] MGCs present some additional advantages over sintered eutectic ceramics, derived from their greater microstructure homogeneity and stability, absence of porosity, and excellent chemical bonding between phases. In addition, the phases in the eutectics are aligned along the growth direction.[2] These ordered microstructures are also intended to produce materials with unusual optical and transport properties,[3,4] substrates for the growth of patterned high-critical-temperature superconductor thin films,[5] and functional ceramics with improved mechanical properties.[6] Moreover, Al_2O_3 based MGCs show high tensile strength and fracture toughness at room temperature, as well as good retention of these properties up to temperatures near the eutectic point.[7,8] Heat and oxidation resistance make these materials very promising to overcome the intrinsic limits of metal and ceramic devices for high efficiency power-generation systems.[9]

Although not exclusively, in most cases the LFZ method has been applied to cylindrical geometry. Laser beams approximating the form of a ring are focused on the surface of a cylindrical precursor to produce a small melt volume. Grown material is pulled out from this

* Corresponding author.
E-mail address: alarrea@posta.unizar.es (A. Larrea).

0955-2219/01/$ - see front matter
PII: S0955-2219(01)00279-5

melt. Cylindrical bars of diameter up to several millimetres and, in principle, unlimited length can be grown in this way. The cylindrical geometry is not suitable for many applications, however, and severe restrictions are found when large surfaces of eutectic material are required.

This paper reports on a study of a different approach, which makes use of an alternative in-plane geometry to overcome the latter constraints. The procedure is similar to that of bead-on-plate welding, where the work-piece surface is scanned by a heating laser source. The surface material layer around the incident beam is melted. The work-piece is traversed under the heating beam and a large surface area can then be processed. An evident advantage of this procedure over LFZ cylindrical treatment is the possibility of preparing large sample areas of eutectic material grown by directional solidification. The main disadvantage is the difficulty in producing the planar and stable solidification fronts necessary for fine and homogeneous eutectic microstructures. This is a consequence of the fact that the melt is not self-sustained as in the float zone melting crystal growth. Instead it lies over a substrate material which perturbs the solidification front.

Using surface heat scanning with a CO_2 laser beam, layers of the ZrO_2/Al_2O_3 binary MGC have been prepared. Its structure consists of continuous interpenetrating networks of single-crystal Al_2O_3 and single-crystal ZrO_2 without grain boundaries. Eutectics of this composition have been chosen for this study because, besides their excellent mechanical properties and chemical stability, these composites have a high melting point ($\approx$1860°C) and relatively simple microstructure. Their growth habits have also been thoroughly studied.[10]

Our aim is, using this eutectic composite, to increase our knowledge about the capabilities of this growth method. The third component, Y_2O_3, which would be required to take full advantage of the excellent mechanical properties of ZrO_2-Al_2O_3 composites by stabilising the zirconia phase has not been added in order to eliminate one possible source of perturbation of the growth. For this purpose, we have studied the structure of the component phases, the microstructure orientation, solidification front and residual thermostresses, both along the scanned surface and transverse sections, using electron microscopy and microspectroscopic techniques. The dependence of the eutectic microstructure on depth from surface, substrate thickness and amount of heat input from the laser source is discussed.

2. Experimental details

2.1. Precursor preparation

Precursors were prepared using commercially available 37% mol of Z_{rO_2} (Alfa, 99%) and 63% mol of Al_2O_3 (Aldrich, 99.99%), corresponding to the eutectic composition. Traces of chromium impurity always present in commercial alumina were enough to enable piezospectroscopic measurements. Powders were milled using a vibratory mill (model MM2000, Restch, Haan, Germany), mixed and uniaxially pressed into a rectangular base pellet. This pellet was sintered in a tube furnace (model HTG, manufactured by CHESA, Madrid, Spain), at 1500°C during 20 h, in an open-ended commercial 99.9% alumina tube. Heating was performed at a rate of 600°C per h, while the sintered pellet was allowed to cool within the furnace following a power cut off at the sintering temperature. This sintered pellet was used as the preform in the following laser induced zone melting experiment.

2.2. Laser zone melting

The eutectic preform was placed on top of an X–Y moving stage apparatus (Integración y Control, Zaragoza, Spain) to which a CO_2 laser (LaserQuanta, Madrid, Spain) was introduced from the outside through reflections in several flat, gold-coated Cu mirrors manufactured in-house. The final focused beam was shaped with an in-house designed and built parabolic mirror, as a long, thin line, measuring about 20 mm in length and 0.5 mm in width. The line appeared symmetrically shaped, with the largest width at its centre. The power density used to melt the eutectic preform was 1 kW cm^{-2}.

Experiments were started from one end of the preform, supported over either Al or Al_2O_3, with the laser line focused perpendicular to the solidification direction, in which it was linearly displaced at speeds of 36 and 72 mm h^{-1}. To allow the solidification front studies referred to later on, frozen melts were obtained by cutting off the laser power before the end of the precursor was reached. Both, the experimental set-up and the shape of the focused laser line are illustrated in Fig. 1.

2.3. Characterisation

The microstructure of the samples was studied using optical microscopy as well as scanning (SEM) and transmission (TEM) electron microscope techniques. SEM experiments in both transversal and longitudinal sample cross-sections (with respect to the growth direction) were performed in a Jeol 6400 microscope. TEM experiments were carried out in a Jeol 2000FXII microscope equipped with a Gatan MSC 794 CCD camera. Thin longitudinal cross-sections were prepared for TEM experiments by mechanically grinding down the specimens to a thickness of 40 μm, followed by further ion milling to electron transparency using low sputtering angles (10°) to minimise differential thinning between the constituent phases.

The Cr^{3+} luminescence and the Raman dispersion measurements were performed under a backscattering

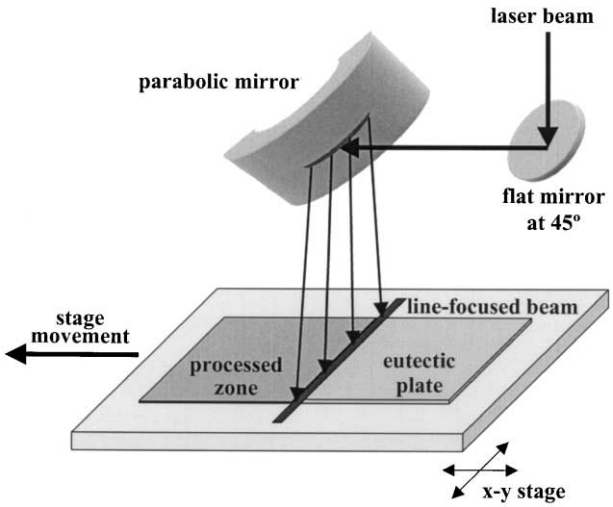

Fig. 1. Experimental setup for the laser zone melting method applied to the growth of the eutectic plates.

geometry, using an optical microprobe spectrometer (Model XY, DILOR, Lille, France) with a diode array multichannel detector. The emission and the Raman dispersion of selected areas can be measured simultaneously with this equipment. A region of about 1 μm diameter and 4 μm in depth can be analysed using a 100× objective lens and 400 μm field aperture in the image focal plane. Further details of the piezospectroscopic technique are given elsewhere.[11]

3. Experimental results and discussion

Sintered ZrO_2–Al_2O_3 eutectic ceramics 0.5–1 mm thick, superficially treated with a CO_2 laser, have been studied. The thickness of the solidified layer ranges from 75 to 250 μm. Obviously, melt layer thickness increases with the amount of heat input (increases with the laser power and decreases with the scanning speed) and decreases when using a metallic support.

The surface of the processed material is smooth and nearly crack free. The alumina–zirconia eutectic surfaces are resistant to failure from propagating cracks. As in the case of LFZ grown fibres, periodic banding is observed on the surface of the solidified sample.[7] In order to study the solidification front the laser power was suddenly switched off several mm away from the ceramic edge. The bulk material rapidly dissipated the heat producing a self-quenching of the molten zone. Unfortunately, this abrupt procedure generated cracks in the frozen volume, which sometimes propagated inside the solidified material but did not perturb the solidification front studies.

3.1. Microstructure

The microstructure of the external surface of the processed layer is presented in Fig. 2, where the dark phase

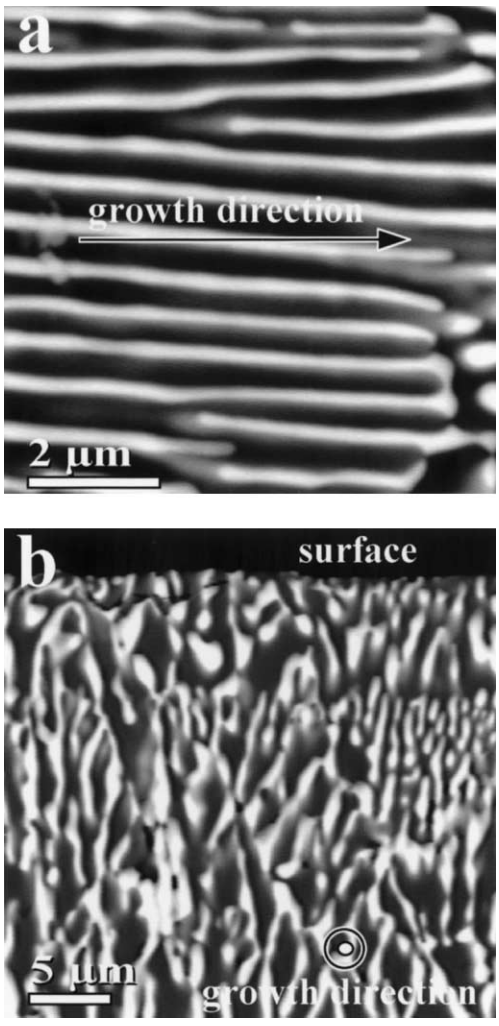

Fig. 2. Laser processed Al_2O_3 (black)–ZrO_2 (white) eutectic ceramic ($V_0 = 72$ mm h^{-1}, Al support). SEM images with backscattered electrons: (a) plane view of the sample surface, (b) transverse cross-section near the surface (the growth direction is perpendicular to the picture).

corresponds to alumina. It consists of large eutectic grains with a very thin microstructure composed of alternate α-Al_2O_3 (~300 nm width) and ZrO_2 (~160 nm width) single crystal meandered lamellae. These lamellae grow perpendicular to the solidification front, i.e. parallel to the processing direction (Fig. 2a) and extend over all the processed area. In the transverse cross-section the microstructure is better described as a uniform distribution of degenerated lamella with a tendency to be oriented perpendicular to the external surface (Fig. 2b).

The total absence of the inconvenient colony structure which has been previously encountered in directionally grown samples[8–12] is also noticeable in these samples. These colonies consist of large, and sometimes faceted, α-Al_2O_3 single crystal grains with inner ordered arrays of small ZrO_2 fibres surrounded by wide boundaries with coarser eutectic microstructure. This colony structure is

usually found in the solidified compounds even for the lowest growth rates reported. Their origin lies in the existence of solidification front instabilities favouring the faceted growth of alumina.[10] On the contrary, the absence of such colonies indicates that the growth of the two component phases is cooperative in our case.

Quenched melts have been observed in order to study the microstructure of the material at different depths from the surface and to correlate the microstructure with the shape of the solidification front. It was thus possible to observe the solid-liquid interface in a longitudinal cross-section (see Fig. 3). The solidification front appeared smooth and no dendrite growth was observed. Absence of a colony structure in the solidified volume and of dendrites in the quenched melt indicated that, in this case, the solidification front was rather regular than cellular.

The solidification front shape is in part determined by the laser radiation absorption in the material. The extinction coefficient of the mixed material for the CO_2 radiation ($\lambda = 10.6$ μm) can be calculated from the volume average of those corresponding to the component phases. Using the room temperature values of the extinction coefficient for Al_2O_3[13] and ZrO_2[14] a value of 650 cm^{-1} was obtained for the eutectic material. This indicated that, in the ceramic precursor at low temperature, 90% of the incoming energy was absorbed in a layer of about 90 μm, similar to the size of the processed area. However, the absorption coefficient of molten oxides is about two orders of magnitude greater than that of the solids at room temperature.[15] Consequently, it is safe to assume that the liquid is opaque to laser radiation, which is completely absorbed within a thin surface layer. The whole molten zone is then formed by heat conduction from the hot exposed surface, producing the smooth penetration profile observed in Fig. 3. The temperature field is stationary in a coordinate frame fixed in the laser beam, although the work-piece moves with a speed V_0. The shape of the solidification front corresponds to the $T = T_m$ stationary isotherm.

A non-planar solidification front shape introduces some changes in the solidification direction and in the solidification rate with respect to the distance to the external surface, modifying in turn the eutectic microstructure. In fact, as shown in the inset of Fig. 3, the lamellae always grow perpendicular to the solidification front. Consequently, they gradually change their orientation from parallel to the external surface, at the top of the processed layer, to perpendicular to the surface at the bottom. Moreover, the spacing between lamellae gradually increases from top to bottom.

The interspacing λ in a solidified eutectic usually depends on the solidification rate R as:[16]

$$\lambda^2 \cdot R = c \tag{1}$$

where c is a constant characteristic of the eutectic material. From Eq. (1) the changes in interparticle distance can be directly related to the changes in growth rates. The change in the size of the microstructure with the distance to the external surface can now be geometrically explained by considering that the scanning direction is not collinear with the direction of growth. Accordingly, as it is illustrated by the model represented in Fig. 4(a), the solidification rate in a given point of the liquid–solid interface is $R(\alpha) = V_0 \cdot \sin\alpha$, where α is the tangent angle of the solidification profile at this point. To test this model the solidification front has been adjusted to a parabolic curve; this curve has been differentiated to get the angle α and then the solidification

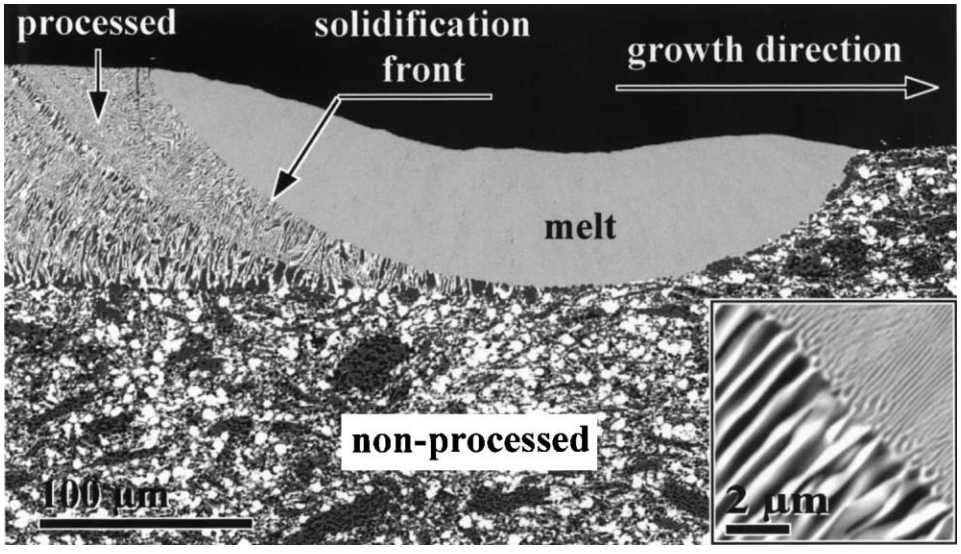

Fig. 3. SEM longitudinal cross-section of a frozen melt ($V_0 = 72$ mm h^{-1} Al support). The inset shows a detail of the interface between the melt and the processed layer.

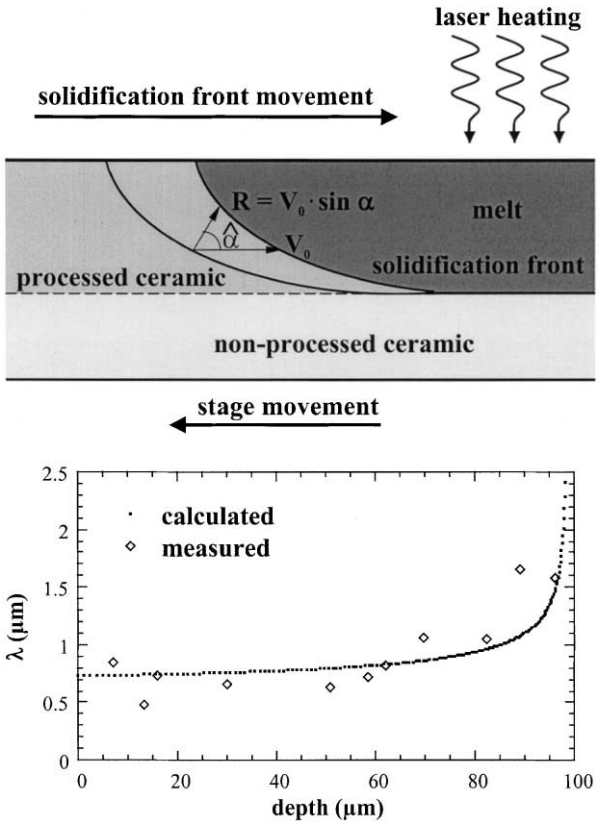

Fig. 4. Top (a) Diagram of the solidification process. The solidification rate at every point (R) is related to the processing rate (V_0) by the tangent angle of the solidification front at this point (α). The angle represented in the picture is the complementary of α. Bottom (b) Interlamellar spacing as a function of distance to the surface ($V_0 = 72$ mm h^{-1}, Al support). Line: calculated from the solidification profile; ◇ experimental measurements.

rate at every point. The calculated interspacing (λ) has been obtained using Eq. (1), where the constant c has been obtained by a least squares fit to the experimental data. Experimental and calculated data are represented in Fig. 4(b), and exhibit a reasonable agreement. The constant $c = 0.9\times10^{-17}$ m^3/s calculated from our experimental data, is also in very good agreement with the value $c = 1\times10^{-17}$ m^3/s reported by Minford et al.[17] for the same compound.

3.2. Crystallography

The crystallography and orientation relationship between the phases has been investigated by TEM techniques in well ordered zones. The eutectic is composed of alternate α-Al_2O_3 ($a = 4.76$ Å, $c = 12.99$ Å, space group $R\bar{3}c$) and monoclinic ZrO_2 ($a = 5.14$ Å, $b = 5.21$ Å, $c = 5.31$ Å, $\beta = 99.22°$, space group $P2_1/c$) single crystals. It has been established by micro-Raman and XRD techniques that the monoclinic is the only zirconia phase present over the whole solidified volume, except in the quenched areas where some tetragonal zirconia was also detected.

The growth directions of the constituent phases have been determined from electron diffraction experiments. As can be seen in Fig. 5, zirconia lamellae grow perpendicular to the $(\bar{1}10)$ plane, whereas those of Al_2O_3 grow along the R-direction: perpendicular to the $(\bar{1}10\bar{2})$ plane.

The orientation relationship is (Z: zirconia, A: alumina):

$$\left(\bar{1}10\right)^Z \sim //\left(\bar{1}10\bar{2}\right)^A \quad \text{and} \quad [111]^Z \sim //\left[02\bar{2}1\right]^A$$

An approximate parallelism is indicated because the zone axis of consecutive ZrO_2 and Al_2O_3 lamellae (as the ones shown in the inset of Fig. 5) are not perfectly parallel, but misaligned $\sim 6°$. Although ZrO_2 solidifies in the tetragonal structure, it suffers a martensitic phase transformation at 1170°C. In conclusion, the zirconia should grow in the $<110>$ cubic direction. The misalignment observed between the monoclinic ZrO_2 and Al_2O_3 axes is caused by the shear deformation during the tetragonal to monoclinic phase transformation.

It is interesting to point out that the growth habit found here differs from the habit commonly observed in directionally solidified zirconia-alumina eutectic compounds along the (0001) Al_2O_3 plane.[7,8,11] In the present case, due to the solidification front morphology, the crystallographic growth direction changes with depth, favouring this R-plane growth habit. To some extent it seems that in our case the growth of the composite is cooperative, which may better accommodate the change in crystallographic orientation produced by the change in solidification direction with depth.

3.3. Piezospectroscopy

The residual stresses are the result of the accommodation of thermal and transformation-induced strains caused by the mismatch in thermal expansion coefficients between both phases as well as the ZrO_2 phase transformation from tetragonal to monoclinic structure. Residual strains modify the mechanical behaviour of the material. In particular they may lead to crack deflection and branching which induces the high fracture toughness of these materials.[6,18] Additionally, the measurement of the residual stress along the sample cross-section is a good tool to explore sample homogeneity and interface morphology.

The residual stresses in the Al_2O_3 phase of the MGC were measured by means of the piezospectroscopic effect in the R-lines luminescence of Cr^{3+} in Al_2O_3, whose maxima exhibit a marked shift as a function of stress.[19] Fig. 6 shows the R-lines measured with the microluminescence set-up along a longitudinal cross-section as compared with those of unstressed ruby obtained under the same experimental conditions. The spectra consist of

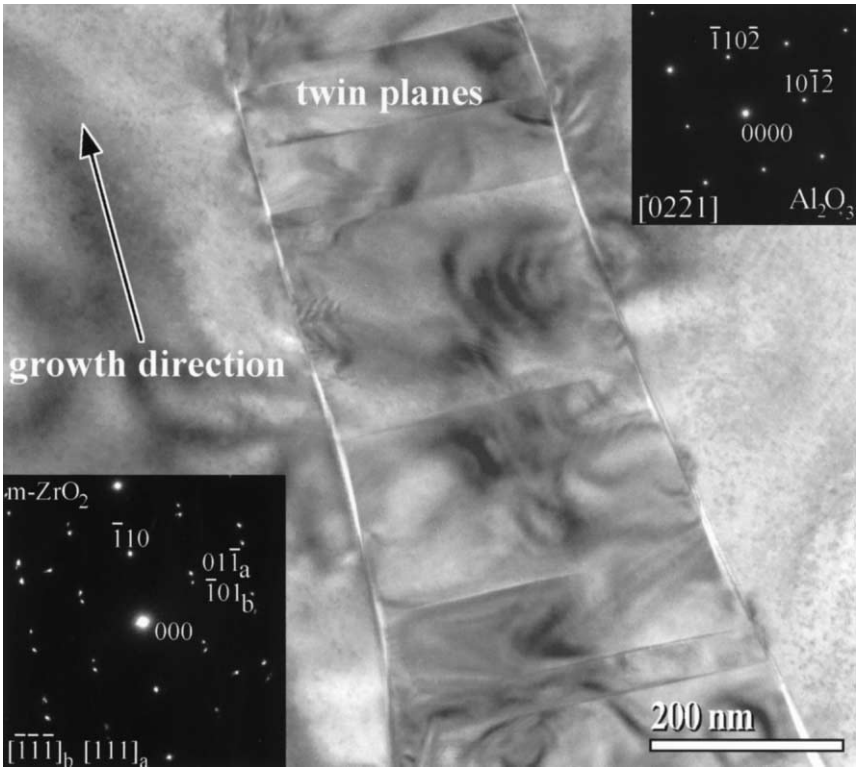

Fig. 5. ZrO_2 lamella between two Al_2O_3 lamellae of a MGP eutectic ($V_0 = 36$ mm h^{-1}, Alumina support). ($\bar{1}10$) Twinning, strains and microcracks at the interface are visible in the TEM image of the longitudinal cross-section. Bottom-left inset: selected area diffraction pattern (SADP) of the ZrO_2 lamella (forbidden spots can be observed due to double diffraction effects). Top-right inset: SADP of the Al_2O_3 lamella. The specimen has to be slightly misaligned ($\sim 6^\circ$) to change from one SADP to the other.

the well-known $R1$ (14 402 cm^{-1}) and $R2$ (14 432 cm^{-1}) lines associated, respectively, to the transitions $\bar{E}(^2E)\rightarrow{}^4A_2$ and $2\bar{A}(^2E)\rightarrow{}^4A_2$ of $Cr^{3+}(d^3)$. Notice the blue shift and broadening of the MGC R-lines in relation to those of ruby.

He and Clarke carried out precise determination of the piezospectroscopic tensors of the *R*-lines emission in ruby under compression.[19] This allows calculating the frequency shift $\Delta\nu$ of the band positions as a function of uniaxial or hydrostatic compressive stress. This always results in a red shift. However, an increase in frequency has been detected in our measurements, which means that the alumina phase in the Al_2O_3–ZrO_2(m) eutectic is in tension. Consequently, ZrO_2(m) is in compression, as it is expected because the tetragonal to monoclinic martensitic phase transition involves an important ZrO_2 cell expansion.

As in the studies conducted in the MGC fibres,[11] we extrapolated the piezospectroscopic tensor for compression into the tensile stresses region. Furthermore, the *R*2-line shift was used to compute approximate values of the hydrostatic stress component (σ_h). This shift was shown to be rather insensitive to the deviatoric stress component. Under this assumption, the following relationship holds:[20]

$$\sigma_h = \frac{\sigma_{11}^* + \sigma_{22}^* + \sigma_{33}^*}{3} \approx \frac{\Delta\upsilon_2}{7.61} \quad (2)$$

where $\Delta\upsilon_2$ refers to the shift of $R2$ (given in cm^{-1}) and σ_{11}^* is the stress tensor component in the $a-$, $m-$, and c-orthogonal axes of the sapphire lattice. σ_h is given in GPa. The hydrostatic stress in Al_2O_3 as determined from the measured $R2$-line shift and Eq. (2) as a function of the distance to the external surface in a longitudinal cross-section is shown in Fig. 7. The average hydrostatic stress values in the sapphire phase are quite uniformly distributed around 400 MPa, down to 150 μm from the external surface. This value is close but lower than that found in the disordered region of the MGC fibres of the same composition grown by LFZ (≈680 MPa).[11] The stress field markedly decreases approaching the ceramic (unstressed) values at the bottom of the melt volume. Notice that lower thermostress values correlate with a wider microstructure. A broadening of the *R*-lines of both ceramic and solidified volume as compared with those of unstressed ruby may also be observed in the spectra in Fig. 6. This broadening is presumably due to the presence of an inhomogeneous stress distribution in the samples.

3.4. Twinning

The main contribution to the thermoelastic stresses studied above stems from the phase transition of the ZrO_2 phase. This phase transition is also evidenced by

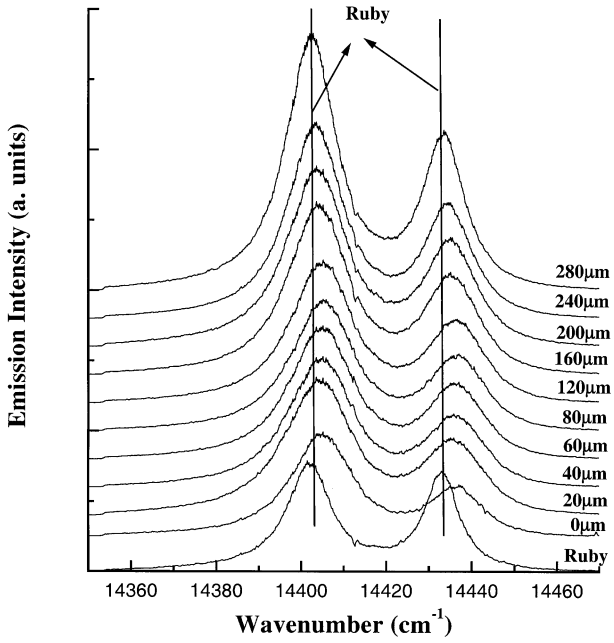

Fig. 6. Cr^{3+} R-line luminescence measured at 300 K with a 100× objective in unstressed ruby and along a line perpendicular to the external surface in a longitudinal cross-section of a 250 μm thick solidified sample ($V_0 = 36$ mm h^{-1}, Alumina support). The distances to the free surface are given in the plot.

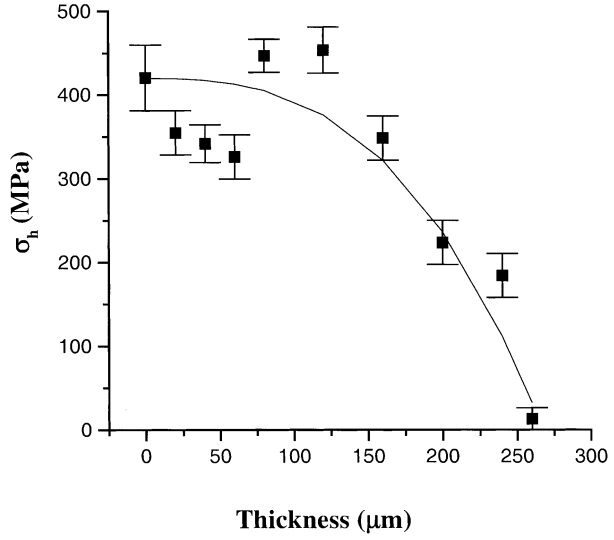

Fig. 7. Experimentally determined values of the hydrostatic mean stress components in Al_2O_3 corresponding to the experiment of Fig. 6.

the presence of twins in the ZrO_2 lamellae in the samples observed by TEM. The appearance of accommodation $(\bar{1}10)$ twins involves the presence of surface relief (a typical behaviour observed in martensitic transformations), producing microcracking at the interface with the alumina lamellae. Both twins and microcracks are clearly visible in Fig. 5.

From symmetry arguments, four orientation variants (twins) are expected in the tetragonal to monoclinic ZrO_2 transformation, but only two are observed. A plausible explanation for this experimental finding is the following. The possible orientation variants after a transformation depend on the point group of the parent phase ($4/mmm$ in tetragonal zirconia), the point group of the martensite ($2/m$ in monoclinic zirconia) and the lattice correspondence (LC) for the tetragonal to monoclinic transformation.[21] From group theoretical calculations it can be deduced that the twinning observed in these samples is only compatible with LC type C ($[100]^t//[0\bar{1}0]^m$ and $[001]^t//[001]^m$)[22], where the second-order symmetry axis of the monoclinic phase is parallel to one second-order symmetry axis of the tetragonal phase and $c_t//c_m$. However, the orientation variants deduced for LC A ($[100]^t//[010]^m$ and $[001]^t//[100]^m$), where c_t is not parallel to c_m, and for LC B ($[100]^t//[0\bar{1}0]^m$ and $[010]^t//[001]^m$), where the second-order monoclinic axis is parallel to the fourth-order tetragonal axis, are not compatible with the orientation variants found in the eutectic. This result is consistent with previous experiments on spherical ZrO_2 particles embedded in an Al_2O_3 matrix, where LC C and (110) twinning was reported.[23] However, these symmetry considerations do not take into account the geometrical constrains experienced by the lamellae during the phase transition. In order to minimise strains, from the four possible orientation variants, the zirconia lamellae display the two variants that present the minimum martensitic expansion along the parallel directions to the lamella: $(\bar{1}10)$ and [111], and the maximum expansion perpendicular to the lamellae: $(11\bar{2})$, where there are no constrains.

4. Conclusions

A procedure for preparing large area plates of composite material grown by solidification techniques is presented. Applied to the growth of eutectic composites, this method allows for the production of very fine and homogeneous eutectic microstructures, which is essential for the achievement of materials with improved mechanical properties. The determination of the processing parameters to obtain such microstructure is one of the main problems in MGC preparation. For the planar geometry used here, the growth habits of the ZrO_2–Al_2O_3 eutectic differ from those encountered in the LFZ grown fibres. The absence of colony structure using this procedure advances the possibility for production of extended coatings with excellent mechanical and chemical properties.

Acknowledgements

The work was financially supported by CICYT (Spain) project MAT 97-0673-C02-01. J.I. Peña is acknowledged for fruitful discussions.

References

1. Waku, Y., Nakagawa, N., Wakamoto, T. and Ohtsubo, H., *Nature,* 1997, **389**, 49–52.
2. Kurtz, W. and Fisher, D. J., *Fundamentals of Solidification*. Trans. Tech. Publications, 1992.
3. Orera, V. M., Peña, J. I., Merino, R. I., Lázaro, J. A., Vallés, J. A. and Rebolledo, M. A., *Appl. Phys. Lett.,* 1997, **71**, 2746–2748.
4. Merino, R. I., Peña, J. I., Orera, V. M. and de la Fuente, G. F., *Solid State Ionics,* 1997, **100**, 313–318.
5. Santiso, J., Laukin, V., Doudkowsky, M., García, G., Figueras, A., Angurel, L. A., Merino, R. I., Peña, J. I., Sanjuán, M. L. and Orera, V. M., *Adv. Mater.,* 2000, **12**, 116–119.
6. Pastor, J. Y., Poza, P., Llorca, J., Peña, J. I., Merino, R. I. and Orera, V. M., *Mater. Sci. Eng*. (in press).
7. Sayir, A., Farmer, S. C., Dickerson, P. O. and H. M. Yun, H. M., *Mat. Res. Soc. Symp. Proc,* 1995, **365**, 21–27.
8. Mazerolles, L., Michel, D. and Perez y Jorba, M. Microstructure and related properties of oriented eutectics involving refractory oxides. In *Studies in Inorganic Chemistry*, eds. R. Metselaar, H. J. M. Heijligers and J. Schaanman. Elsevier, Amsterdam, Vol. 3, 1984, pp. 841–844.
9. Waku, Y. and Sakuma, T., *J. Eur. Ceram. Soc.,* 2000, **20**, 1453–1458.
10. Borodin, V. A., Starostin, M.Yu. and Yalovets, T. N., *J. Crystal Growth.* 1990, **104** 148–1536. Bourban, S., Karapatis, N., Hofman, H., and Kurz, W., *Acta Mater*., 1997, 45, 5069–5075.
11. Pardo, J. A., Merino, R. I., Orera, V. M., Peña, J. I., Gonzalez, C., Pastor, J. Y. and Llorca, J., *J. Am. Ceram. Soc.,* 2000, **83**, 2745–2752.
12. Starostin, M.Yu., Gnesin, B. A. and Yalovets, T. N., *J. Cryst. Growth,* 1997, **171**, 119–124.
13. Gervais, F., In *Handbook of Optical Constants of Solid II,* ed. E. D. Palik. Academic Press, 1991, pp. 761–775.
14. Aleksandrov, V. A., Vasilev, A. B., Kalgin, Yu.A., Kislovskii, L. D. and Tatarintsev, V. M., *Opt. Spectrosc,* 1976, **40**, 627–628.
15. Nason, D. O., Yen, C. T. and Tiller, W. A., *J. Crystal Growth,* 1990, **106**, 221–226.
16. Chalmers, B., *Principles of Solidification*. John Wiley and Sons, New York, 1964.
17. Minford, W. J., Bradt, R. C. and Stubican, V. S., *Journal of the American Ceramic Society,* 1979, **62**, 154–157.
18. Kingery, W. D., Bowen, H. K. and Uhlmann, R. D., *Introduction to Ceramics*, 2nd edn. John Wiley and Sons, New York, 1976.
19. He, J. and Clarke, D.R., *J. Am. Ceram. Soc*., 1995, 78, 1347–1350. He, J., & Clarke, D.R., *Proc. R. Soc. Lond*, 1997, **A453**, 1881–1901.
20. Chai, M. and Brown, J. M., *Geophys. Res. Lett.,* 1996, **23**, 3539–3542.
21. Van Tendeloo, G. and Amelinckx, S., *Acta Crystallogr.,* 1974, **A30**, 431–440.
22. Kriven, W. M., Fraser, W. L. and Kennedy, S. W., In *Advances in Ceramics*, Vol. 3, ed. A. H. Heuer and L. W. Hobbs. The American Ceramic Society, Columbus, OH, 1981, pp. 82–97.
23. Kriven, W. M., In *Science and Technology of Zirconia II*, eds. N. Claussen, M. Ruhle and A. H. Heuer. The American Ceramic Society, Columbus, OH, 1984, pp. 64–77.